Gulf Journal of Mathematics ISSN: 2309-4966
Vol 19, Issue 2 (2025) 340-368 https://doi.org/10.56947/gjom.v19i2.2633

ANALYSIS OF A NOVEL FRACTIONAL-ORDER CHAOTIC CIRCUIT WITH A FEEDBACK MEMRISTOR: DESIGN, DYNAMICS, AND APPLICATION

HAGAR SALMAN[1,2]*, ABASS ABDEL KADER[2] and FATMA KAMAL[2,3]

Abstract. In this research, a novel fractional-order chaotic circuit incorporating a feedback memristor is presented. The structure of the circuit and the associated mathematical model are described in detail. The complex dynamics of the circuit are analyzed using stability analysis, Poincaré maps and numerical simulations, revealing the presence of a saddle fixed point and coexisting attractors. The influence of changing the system variables and initial conditions is studied using bifurcation plots and Lyapunov exponents. The circuit exhibits a variety of nonlinear behaviours including periodic, quasi-periodic, and chaotic dynamics. Furthermore, experimental simulations performed with a chain-ship circuit configuration validate the theoretical results and show strong agreement with the numerical analysis. Finally, a robust sound encryption scheme is presented that exploits the pseudorandom sequences generated by the chaotic memristive circuit.

1. Introduction

Fractional calculus (FC), the class of differentials and integrals to non-integer orders development, was the brilliant notion of Gottfried Leibniz at the end of the 17^{th} century. There are several methods for computing fractional derivations and integrals, including Riemann-Liouville, Caputo, Atangana-Baleanu and Grünwald-Letnikov [42, 49, 16, 29]. The topic has been used primarily in a mathematical framework, but in recent years FC has been recognized as an effective approach for studying and modeling a variety of real-world problems, for example in biology [37], economics [25], finance [32], chemistry [30], physics [11], mechanics [40], epidemiology[8] and engineering [53].

Currently, when modeling and analyzing real engineering systems, differential equations are typically viewed as equations of integer order. However, some real-world engineering systems display dynamic phenomena of fractional order due to their structural, physical and chemical characteristics. For example, real capacitors and inductors exhibit characteristics of dissipation effects such as: thermal

Date: Received: Jan 20, 2025; Accepted: Feb 12, 2025.
* Corresponding author.
2020 *Mathematics Subject Classification.* Primary 37D45, 34A08; Secondary 37M05, 94A60, 65P20.

Key words and phrases. Fractional differential equations, Nonlinear circuits, Memristors, Chaos, Bifurcation, Sound encryption.

memory, internal friction, ohmic friction, and nonlinearity [6, 38, 3, 50]. As a result, their underlying electrical properties can be more accurately described by frationary models [47]. In recent decades, the area of electrical engineering has made extensive use of the fractional derivative, including research in control theory [2, 44, 56, 57] and circuit theory [70, 51, 7, 67, 41]. Interest in the research of models of memristors, capacitors, and inductors in fractional order, particularly in circuit analysis is rising, where a fractional representation of the entire system is created by integrating fractional calculus into the circuits.

The memristor is a nonlinear electrical component with two terminals that links the magnetic flux and the electrical charges [65]. Furthermore, the memristor can recall previous voltages or currents and has a dynamic relationship with them, unlike a linear (or nonlinear) resistor. To be more precise, a memristor's resistance drops when the flow of current is in one direction and vice versa [45]. Despite interruptions in current flow, the memristor maintains its final state, leading to the i–v characteristic curve of memristor, which is compressed to the origin in the form of a hysteresis loop. Among memristive elements, this is one of their best known characteristics controlled by periodic bipolar signals of arbitrary amplitudes and frequencies [21].

The developed Chua's ideal memristor in [20] was mostly of theoretical relevance. The ideal memristor's model, which is not universal and generalisable since it considers fewer elements, is the basis for several introduced models, such as: the spice macromodel [14, 13] and the flux-controlled model [9, 10]. This makes it difficult to create circuits for real-world applications. Meanwhile, real devices were modelled as memristors using the extended or generic memristors that Chua and Kang first proposed in 1976. [22]. Therefore, memristor had received little attention until the first ten years of the twenty-first century ended. In 2008, a team from HP Laboratories created the first passive memristor that is electronic [63]. In addition, KNOWM Inc. memristors have been commercially available for five years [17]. Numerous applications, including analog circuits [12, 43], signal processing [61, 27], neural networks [4, 69], and chaotic systems [1, 59], have made use of memristors. According to previously established theories, the intrinsic nonlinearity of the memristor modeled in fractional calculus may be used to create new chaotic circuits and complexly dynamic systems. In this direction, memristive chaotic systems of fractional order are reported in [31, 33, 55, 39].

This paper proposes an innovative fractional-order chaotic circuit design, which includes a memristor model described in [68] as a feedback signal. The circuit design and mathematical model of the new circuit are introduced. The qualitative behaviour of the suggested system is reported using Lyapunov exponents, bifurcation diagrams, Poincaré maps, stability analysis of fixed points, and phase portraits. Depending on the system parameters values, the proposed system exhibits complex dynamics as periodic, quasi-periodic, and chaotic motion. The experimental implementation is provided to the new circuit. Moreover, the system's chaotic behaviour is utilised to present a reliable sound encryption algorithm.

The remaining part of the research is arranged as follows: Section 2 shows the needed preliminaries in this work. Section 3 deals with the mathematical reproduction of the proposed circuit, which is obtained and developed to study the system dynamics. The proposed system dynamical characteristics, influence of parameters and numerical simulations are examined in section 4. Section 5 shows the realization and experimental simulation of the proposed circuit. The encryption and decryption process of sound data based on the pseudo-random numbers that result from the proposed system is described in section 6. At last, the results of the research are outlined in section 7.

2. Preliminaries

Certain definitions associated with (FC), stability criterion and memristors are reviewed briefly in this section.

Definition 2.1. Fractional derivatives are defined and approximated in a variety of techniques as illustrated in [58]. The most suitable fractional operator for simulating real-world phenomena is the Caputo derivative due to its flexibility in analysis. Caputo derivative addresses initial and boundary value problems and is utilized to model situations that consider past interactions as well as problems exhibiting non-local characteristics. Caputo definition is given by [58]

$$ {}_{0}^{c}D_{t}^{\alpha} f\left(t\right) = \frac{1}{\Gamma\left(1-\alpha\right)} \int_{0}^{t} \left(t-s\right)^{-\alpha} f^{(1)}\left(s\right) ds, \tag{2.1} $$

where $0 < \alpha \leq 1$, $t \geq 0$, and the function $\Gamma(.)$ is considered as the Gamma function

$$ \Gamma(z) = \int_{0}^{\infty} t^{z-1} e^{-t} dt. \tag{2.2} $$

Definition 2.2. For a dynamical system of fractional order that is expressed as

$$ {}_{0}^{c}D_{t}^{\alpha} x(t) = f(t, x(t)), \qquad x(t) \in \mathbb{R}^{n} \tag{2.3} $$

is claimed to have an unstable fixed point at x_O when

$$ {}_{0}^{c}D_{t}^{\alpha} x(t) = f(t, x_O(t)) = 0, \tag{2.4} $$

if and only if $\left|arg\left(\lambda_k\left(J\right)\right)\right| < \alpha\pi/2,\ \ k = 1, 2, .., n$ where J donates the Jacobian matrix of $f\left(x_O\right)$ and λ_k are considered as the eigenvalues of J, as shown in Fig. 1. If one of the eigenvalues $\lambda_1 < 0$ and the other $\lambda_2 > 0$, then it is called a saddle point when equilibrium has been reached [5].

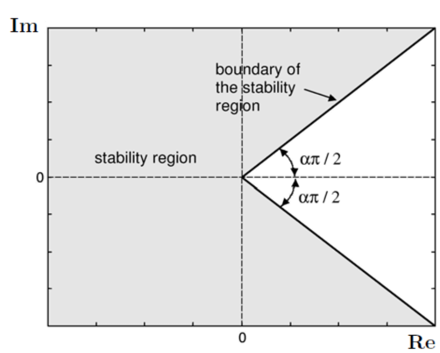

Figure 1. Region of stability for the system of fractional order.

Definition 2.3. The generalised interpretation of a memristor was given by Chua and Kang [22] as follows

$$\begin{aligned} z(t) &= G(y, x, t)x(t), \\ \dot{y}(t) &= F(y, x, t), \end{aligned} \tag{2.5}$$

where the state variable of the memristor is denoted by $y(t)$, while $x(t)$ and $z(t)$ represent the input and output of the memristor, respectively. $F(.)$ and $G(.)$ indicate functions pertaining to the particular memristor.

3. Mathematical representation of the proposed fractional circuit

Starting from the memristor model that was introduced in [68], the voltage-controlled memristor is expressed as

$$\begin{aligned} i_M &= (aw^2 - b)v_M, \\ \dot{w}(t) &= -cv_M - dw + ev_M^2 w, \end{aligned} \tag{3.1}$$

where i_M and v_M indicate the current and voltage flowing through the memristor, respectively, with a, b, c, d, and e are identified as constants related to the memristor.

In the new proposed circuit as shown in Fig. 2, u_1, u_2 and u_3 are equal to $-V_{c_1}$, $-V_{c_2}$ and $-V_{c_3}$, respectively. The memristor is charged by voltage across it v_M equals to u_3, and the electrical input current of resistor R_a is the memristor current, so it is found that

$$\begin{aligned} {}_0^cD_t^\alpha V_{c_1} &= \left(\frac{1}{R_1c_1}\right)V_{c_2}^2 - \left(\frac{1}{R_2c_1}\right)V_{c_1}, \\ {}_0^cD_t^\alpha V_{c_2} &= -\left(\frac{1}{R_3c_2}\right)V_{c_3}, \\ {}_0^cD_t^\alpha V_{c_3} &= \left(\frac{1}{R_4c_3}\right)i_MR_a + \left(\frac{R_7}{R_6}\right)\left(\frac{1}{R_5c_3}\right)V_{c_2}. \end{aligned} \tag{3.2}$$

These capacitors possess identical values ($c_1 = c_2 = c_3 = c$), also ($R_1 = R_2 = R_3 = R_4 = R$). Let V_{c_1} is considered as x, V_{c_2} is considered as y, V_{c_3} is considered as z, $\tau = t/Rc$, $p = R_7/R_6$, $i_M = -(aw^2 - b)V_{c_3}$ and $\dot{w}(t) = cV_{c_3} - dw + eV_{c_3}^2 w$. The new dimensionless memristive non-integer order system shown in Fig. 2 can be mathematically modeled as

$$\begin{cases} {}_0^cD_\tau^\alpha x = y^2 - x, \\ {}_0^cD_\tau^\alpha y = -z, \\ {}_0^cD_\tau^\alpha z = -azw^2 + bz + py, \\ {}_0^cD_\tau^\alpha w = cz - dw + ez^2w, \end{cases} \tag{3.3}$$

where a, b, c, d, and e in this formula represent the memristor's coefficients, while p is a parameter depends on the circuit's elements.

4. Dynamical analysis

This part covers the theoretical and numerical simulations dynamics of the proposed system in (3.3)

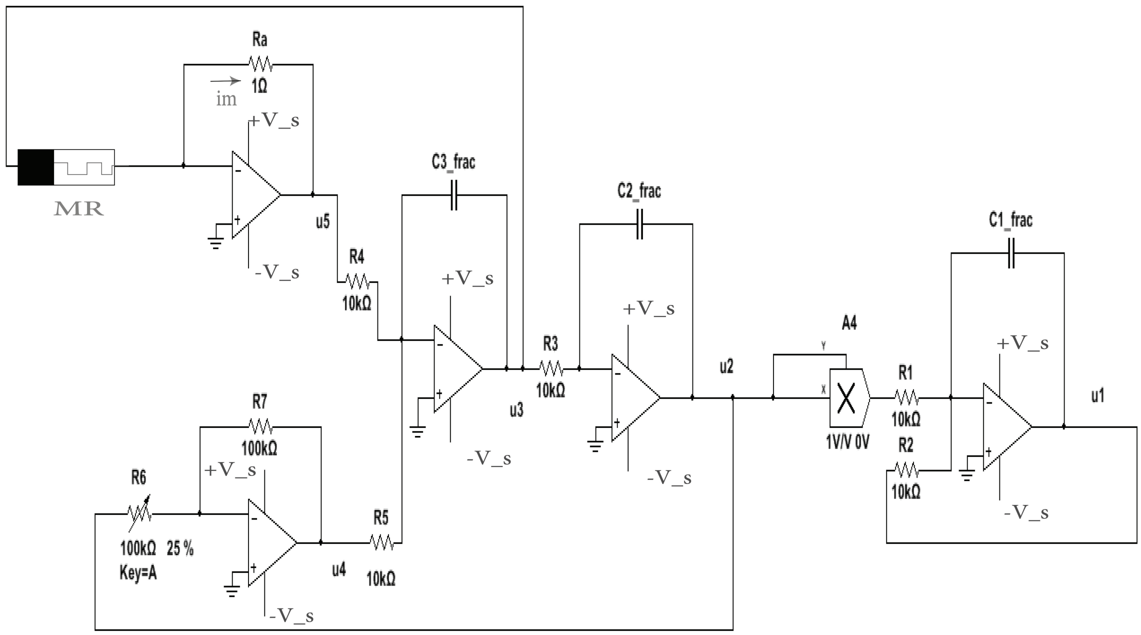

FIGURE 2. The new proposed fractional-order memristive circuit.

4.1. **Dissipation analysis.** The proposed system in (3.3) shows divergence as follows

$$\nabla V = \frac{\partial \dot{x}}{\partial x} + \frac{\partial \dot{y}}{\partial y} + \frac{\partial \dot{z}}{\partial z} + \frac{\partial \dot{w}}{\partial w} = -1 - aw^2 + b - d + ez^2. \tag{4.1}$$

When the values of the system parameters a, b, d, e, and the initial condition are assigned as 0.1, 0.5, 10, 4, and $(0, 5, 0, -0.1)$, respectively, while V refers to the phase volume, it has been found that the $\nabla V < 0$, which signifies that the state of the proposed system can solely change by a limited amount and the system exhibits dissipation, indicating that the attractors might have chaotic characteristics.

4.2. **Stability analysis using Routh-Hurwitz criterion.** The proposed system in (3.3) has a Jacobian matrix linearization given as

$$J = \begin{bmatrix} -1 & 2y & 0 & 0 \\ 0 & 0 & -1 & 0 \\ 0 & p & -aw^2 + b & -2azw \\ 0 & 0 & c + 2ezw & -d + ez^2 \end{bmatrix}. \tag{4.2}$$

The system has a characteristic equation defined as

$$\lambda^4 + S_1\lambda^3 + S_2\lambda^2 + S_3\lambda^1 + S_4 = 0, \tag{4.3}$$

where the coefficients S_1, S_2, S_3, and S_4 depend only on the system parameters and specified as

$$\begin{aligned}
&S_1 = aw^2 - ez^2 - b + d + 1,\\
&S_2 = d - b + p - bd + aw^2 - ez^2 + adw^2 + bez^2 + 2acwz + 3aew^2z^2,\\
&S_3 = p - bd + dp - epz^2 + adw^2 + bez^2 + 2acwz + 3aew^2z^2,\\
&S_4 = -epz^2 + dp.
\end{aligned} \tag{4.4}$$

Based on Routh-Hurwitz criterion [5] the stability of a fraction-order system is achieved when

$$\begin{aligned}
&S_1 > 0,\\
&S_2 > 0,\\
&S_3 > 0,\\
&S_4 > 0,\\
&S_2S_3 > S_1S_4.
\end{aligned} \tag{4.5}$$

These conditions ensure all eigenvalues have negative real parts, guaranteeing stability.

The system features a single equilibrium point $O\,(0,0,0,0)$, and the Jacobian matrix corresponding to point O is

$$J_O = \begin{bmatrix} -1 & 0 & 0 & 0 \\ 0 & 0 & -1 & 0 \\ 0 & p & b & 0 \\ 0 & 0 & c & -d \end{bmatrix}. \tag{4.6}$$

For p, b, c, and d have been set to 4, 0.5, 0.5,and 10, respectively, the eigenvalues are $\lambda_1 = -10$ *and* $\lambda_2 = -1$ *and* $\lambda_{3,4} = 0.35 \pm 1.9691j$. With the aid of Definition 2 in Sec. 2, it is necessary for the fractional system (3.3) to keep at least one eigenvalue λ_k within the unstable zone,i.e, $|arg\,(\lambda_k\,(J))| < \alpha\pi/2$ to stay chaotic, which means that for the system to exhibit chaotic behaviour $\alpha > 0.8874$ and O is a saddle equilibrium point.

4.3. **Lyapunov exponent, Kalpen-York dimension and Poincaré section.** Mathematically, exponents of Lyapunov are calculated by averaging the exponential divergence between neighbouring pairs of trajectories in phase space. In other words, they tell us how quickly the distance between two points in a system grows. Computing Lyapunov exponents can be complex and computationally intensive, but it is a crucial tool for comprehending the dynamics of chaotic systems. In this work, the algorithm of Wolf et al [66, 26] is used for calculating the Lyapunov exponents of the proposed system at α, a, b, p, c, d, e, and initial condition equal to 0.98, 0.1, 0.5, 4, 0.5, 10, 4, and $(0, 5, 0, -0.1)$, respectively. The four Lyapunov exponents are $L_1 = -1.0547$, $L_2 = 0.2635$, $L_3 = -0.0509$ and $L_4 = -4.1137$. The positive Lyapunov exponent value indicates that the proposed system in (3.3) is chaotic and extremely sensitive to initial conditions.

The dimension of the attractor is represented by Kalpen-York dimension [66], which is defined as the following

$$D_{KY} = j + \frac{1}{|L_{j+1}|}\sum_{t=1}^{j} L_t\ , \tag{4.7}$$

TABLE 1. The characteristics of coexisting attractors in various conditions.

Property	Parameter	Initial conditions	Figure
Chaotic Attractor	$a = 0.1$, $b = 0.5$, $p = 4$, $c = 0.5$, $e = 4$, $d = 10$, and $\alpha = 0.98$	$(0, \pm 5, 0, \mp 0.1)$	Figs. 4a and 4b
Quasi periodicity	$a = 0.1$, $b = 0.5$, $p = 2$, $c = 0.5$, $e = 4$, $d = 10$, and $\alpha = 0.98$	$(0.1, \pm 9, 0, \mp 0.3)$	Figs. 4c and 4d
Period 1 attractor	$a = 1$, $b = 0.5$, $p = 4$, $c = 0.5$, $e = 4$, $d = 10$, and $\alpha = 0.98$	$(0.1, \pm 0.1, 0, \mp 0.3)$	Figs. 4e and 4f
Period 2 attractor	$a = 0.1$, $b = 0.5$, $p = 4$, $c = 1$, $e = 4$, $d = 10$, and $\alpha = 0.98$	$(0.3, \pm 0.3, 0, \mp 0.3)$	Figs. 4g and 4h
Symmetrical chaotic	$a = 0.1$, $b = 0.5$, $p = 4$, $c = 0.5$, $e = 4$, $d = 10$, and $\alpha = 0.9$	$(2, \pm 9, \mp 0.3, 0)$	Figs. 4i and 4j

where j is taken into account as the largest integer given that $\sum_{t=1}^{j} \geq 0$ and $\sum_{t=1}^{j+1} \leq 0$.
The Kalpen-York dimension of the system (3.3) at $p = 4$ and $\alpha = 0.98$ is $D_{KY} = 2.1374$, proving that the new introduced memristive system (3.3) has a fractal dimension, and the existence of chaotic attractors has also been proven.

A Poincaré map represents points in phase space that are stroboscopically sampled or observed at equal time intervals. For a, b, c, d, and e equal to 0.1, 0.5, 0.5, 10, and 4, respectively, the Poincaré map of proposed system in (3.3) at $p = 4$ displayed in Fig. 3a shows a chaotic structure, characterized by an irregular, non-periodic point distribution. This confirms sensitivity to initial conditions and complex dynamics, which is a signature of deterministic chaos. The system's nonlinearity is further showcased by the clustering of points in certain regions, which also suggests the possibility of chaotic attractors. The closed-loop trajectory in the Poincaré map of Fig. 3b at $p = 2.8$ indicates the existence of a periodic orbit in this system. In fact, its regular and smooth structure confirms no chaotic behaviour at all, showing this dynamic regime to be stable and predictable. This periodic behaviour reflects the convergence of the system to a limit cycle under the given parameters.

4.4. **Symmetrical coexisting attractors.** The system presented in equation (3.3) exhibits symmetry around the $x-axis$, a property that can be deduced from invariance when changing (x, y, z, w) to $(x, -y, -z, -w)$, as shown in equation (4.8)

$$\begin{cases} {}_0^cD_\tau^\alpha x = y^2 - x, \\ {}_0^cD_\tau^\alpha y = -z, \\ {}_0^cD_\tau^\alpha z = -azw^2 + bz + py, \\ {}_0^cD_\tau^\alpha w = cz - dw + ez^2 w \end{cases} \Rightarrow \begin{cases} {}_0^cD_\tau^\alpha x = y^2 - x, \\ -{}_0^cD_\tau^\alpha y = z, \\ -{}_0^cD_\tau^\alpha z = azw^2 - bz - py, \\ -{}_0^cD_\tau^\alpha w = -cz + dw - ez^2 w. \end{cases} \tag{4.8}$$

Fig. 4 illustrates the typical coexisting attractors of this system, with the blue and red paths representing the phase diagrams of the system, originating from symmetrical initial conditions with identical parameter sets. Table 1 presents different states of system (3.3) along with their respective parameters, initial conditions, and figure references in Fig. 4.

4.5. **Influence of the parameters.**

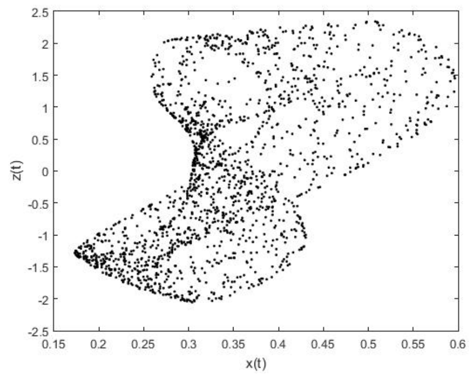

(A) Poincaré map at $p = 4$.

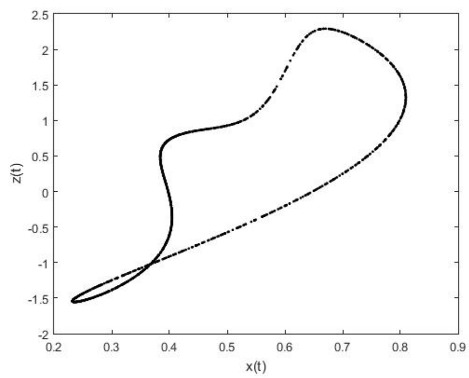

(B) Poincaré map at $p = 2.8$.

FIGURE 3. Poincaré map of the system (3.3) in $x - z$ plane at $\alpha = 0.98$ and initial conditions $(0, 5, 0, -0.1)$.

4.5.1. *Bifurcation analysis.* As the variable a is changed from 0 to 1, the bifurcation diagram Fig. 5a explains the system's transitions and its variations. It shows dense clusters at the start signifying multi-stable or quasi-periodic dynamics that is further followed by period doubling bifurcations which leads to chaos ($0 < a < 0.18$). The chaotic regions consist of continuous and irregular bands with system windows where periodic behaviour emerges and chaos is interrupted. The system further stabilizes for larger a values ($a > 0.45$) by converging to fixed or periodic points which reduces chaos. Fig. 5b presents the largest Lyapunov exponent corresponding to the bifurcation diagram, confirming chaos where the exponent is positive and periodicity where it approaches zero. The highlight of this result is the transition of the system from multi-stability to chaos and finally back to stability, where this is very sensitive to parameter interaction in periodicity and chaos, which becomes very important for control and predictability in applications.

The bifurcation of parameter b with the system and its corresponding Lyapunov spectrum portraits are given in Figs. 6a and 6b, respectively. This bifurcation diagram illustrates the dynamics of the system for parameter values of b lying

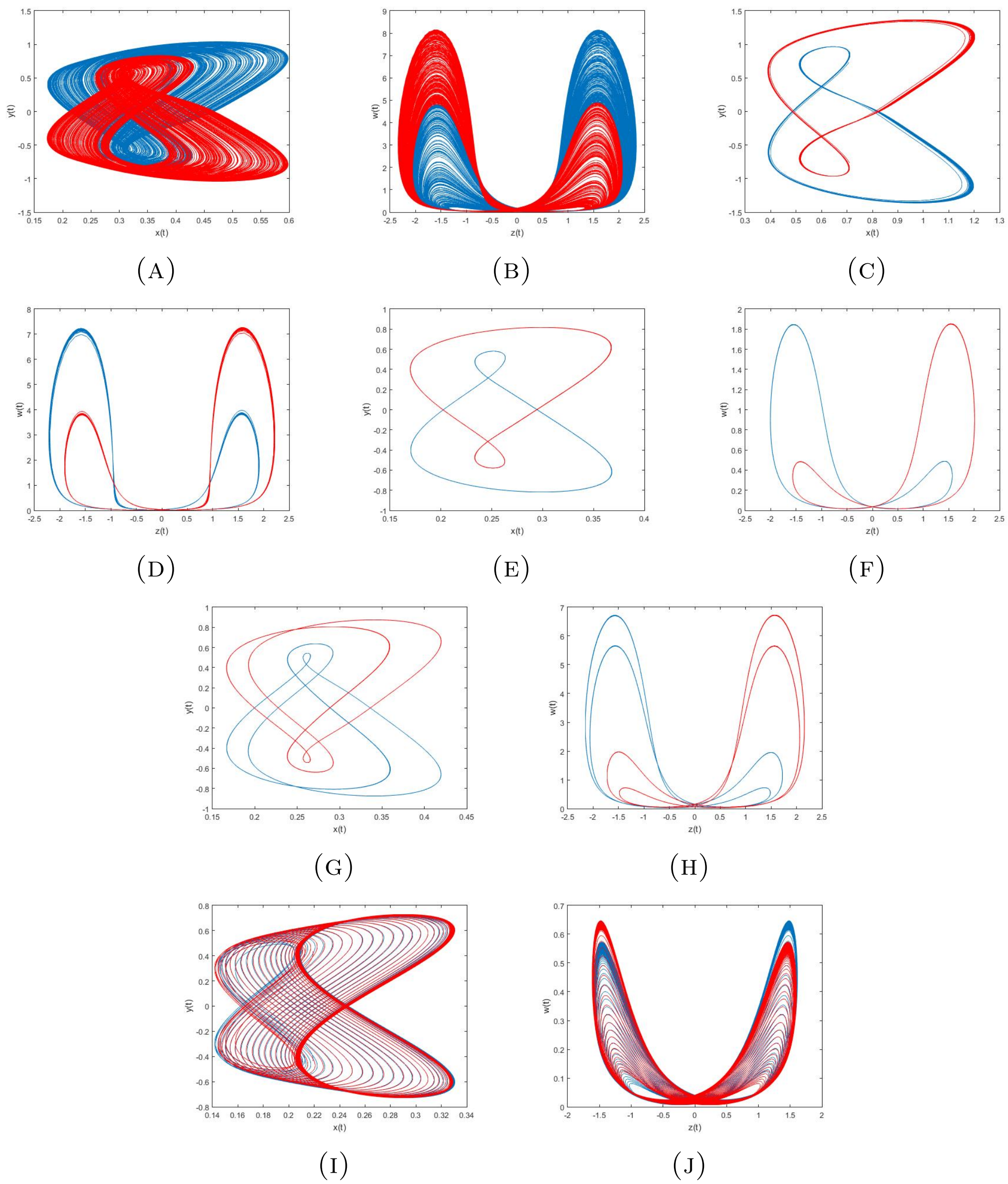

FIGURE 4. Symmetrical coexistent attractors of the system on the $x - y$ and $z - w$ plane.

between 0 and 1, wherein clustering begins near $b = 0.1$, indicating multi-stable or quasi-periodic states. As b increases, the presence of period-doubling bifurcations ($0.2 \leq b \leq 0.45$), which subsequently leads to chaos ($0.45 < b \leq 0.8$), is recognized from densely packed points in the diagram under these states, demonstrating great dependence on initial conditions. Periodic windows interspersed within the chaotic band indicate transitory stabilizations before a reversion into chaos, yet until higher b values (> 0.8) with the diminished bifurcations signify periodic behaviour stabilization of the system. The result emphasizes the variety of dynamical transitions and the sensitivity of the system to parameter b,

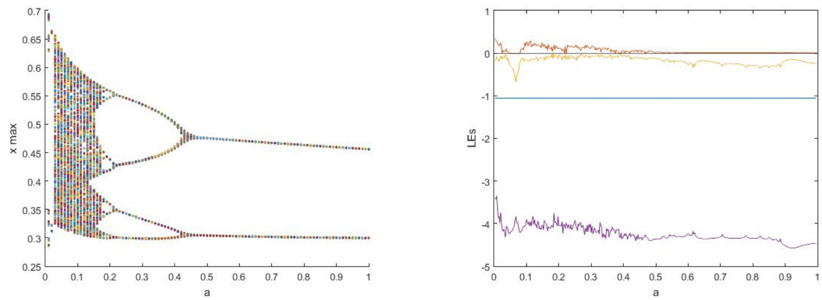

(A) (B)

FIGURE 5. Bifurcation of parameter $a \in [0, 1]$ at $c = 0.5$, $e = 4$, $b = 0.5$, $p = 4$, $d = 10$, and $\alpha = 0.98$ with initial conditions given by $(0, 5, 0, -0.1)$: **(a)** Bifurcation of a with xmax of system (3.3), **(b)** Bifurcation of a with LEs of system (3.3).

whose routes range from multi-stability through chaos and periodic stabilization; this knowledge is of utmost importance for applications with control over the behaviour.

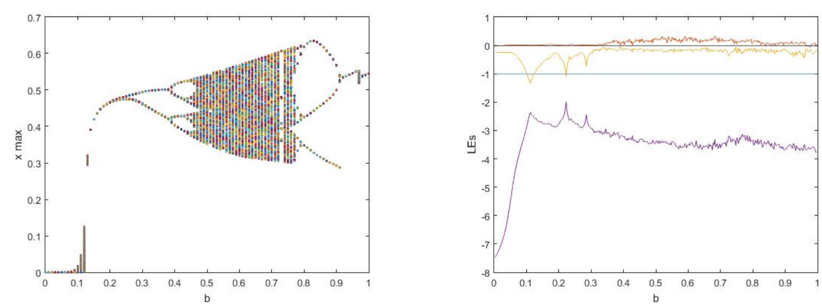

(A) (B)

FIGURE 6. Bifurcation of parameter $b \in [0, 1]$ at $c = 0.5$, $e = 4$, $a = 0.1$, $p = 4$, $d = 10$, and $\alpha = 0.98$ with initial conditions given by $(0, 5, 0, -0.1)$: **(a)** Bifurcation of b with xmax of system (3.3), **(b)** Bifurcation of b with LEs of system (3.3).

The parameter c bifurcation with the system is depicted in Fig. 7a, showing the variation in the system behaviour as $c \in [0, 1.5]$. For small values of c (around $c = 0.1$), the system displays densely packed points, indicating chaos state. As c increases, period-doubling bifurcations appear temporary stabilization ($0.1 < c < 0.3$) before transitioning back to chaos, after that points begin clustering strongly, indicating chaotic dynamics again. In the interval after $c \approx 0.55$, the chaos is temporarily structured with very stable regions in between called periodic windows, until a larger c near 1.5 stabilizes into distinct periodic attractors. The Lyapunov spectrum bifurcation in Fig. 7b confirms the result obtained from The parameter c bifurcation with the system, as the exponent is positive where chaos exists and approaches zero where periodicity happens. This result underscores the system's sensitivity to parameter c, with transitions between chaos and periodicity exhibiting organized periodic windows to stabilization, which is very important for understanding and controlling dynamic behaviour.

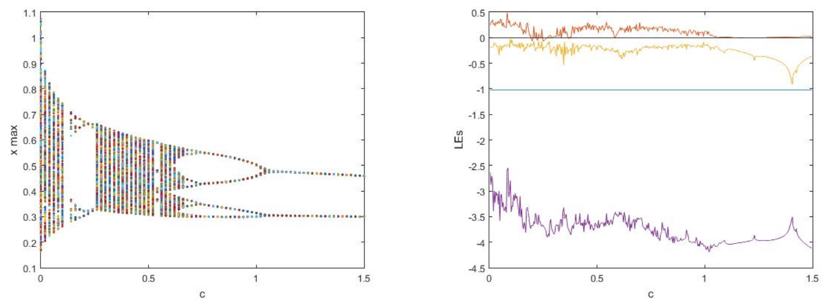

(A) (B)

FIGURE 7. Bifurcation of parameter $c \in [0, 1.5]$ at $a = 0.1$, $e = 4$, $b = 0.5$, $p = 4$, $d = 10$, and $\alpha = 0.98$ with initial conditions given by $(0, 5, 0, -0.1)$: **(a)** Bifurcation of c with xmax of system (3.3), **(b)** Bifurcation of c with LEs of system (3.3).

The influence of changing parameter $d \in [5, 15]$ on system (3.3) is determined by the parameter bifurcation with the system shown in Fig. 8a and with the Lyapunov spectrum shown in Fig. 8b, where it is clear that the proposed system behaves chaotically when $(5 < d < 11)$. Beyond $(d \approx 10)$, the system shows intermittent regions of periodic windows amidst chaotic behaviour, eventually stabilizing into distinct periodic attractors for larger values of (d) near 15. This result highlights the system's chaotic behaviour for $d \in [5, 15]$, with intermittent periodic windows and eventual stabilization, demonstrating the parameter's critical role in controlling chaos and periodicity.

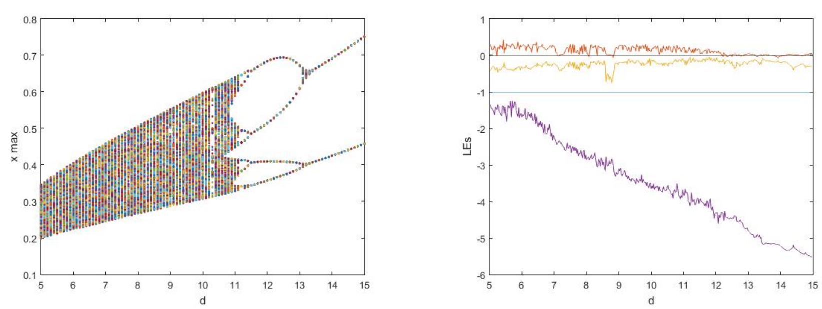

(A) (B)

FIGURE 8. Bifurcation of parameter $d \in [5, 15]$ at $a = 0.1$, $e = 4$, $b = 0.5$, $p = 4$, $c = 0.5$, and $\alpha = 0.98$ with initial conditions given by $(0, 5, 0, -0.1)$: **(a)** Bifurcation of d with xmax of system (3.3), **(b)** Bifurcation of d with LEs of system (3.3).

To investigate the effect of changing parameter $e \in [1, 7]$ on system (3.3), the bifurcation of the parameter e with the system and the corresponding portrait of the Lyapunov spectrum are shown in Figs. 9a and 9b, respectively, where they capture the system's behaviour as parameter e varies from 1 to 7. In Fig. 9a, at lower values of e, the system exhibits a single stable branch, indicating a periodic state. As e increases ,approximately $(2 < e < 3)$, the diagram reveals the emergence of multiple branches, suggesting the onset of period-doubling bifurcations and the transition to chaotic dynamics. Beyond $(e \approx 3.5)$, the system shows intermittent regions of periodic windows amidst chaotic behaviour, eventually stabilizing into organised chaotic attractors for larger values of e near 7. The diagram illustrates the changing parameter in an effective manner. The sensitivity of the system to parameter changing is considered to be very high and shows the interplay between periodicity and chaos. This diagram provides great insight into the dynamical behaviour of the system and its sensitivity to parameter e change conditions.

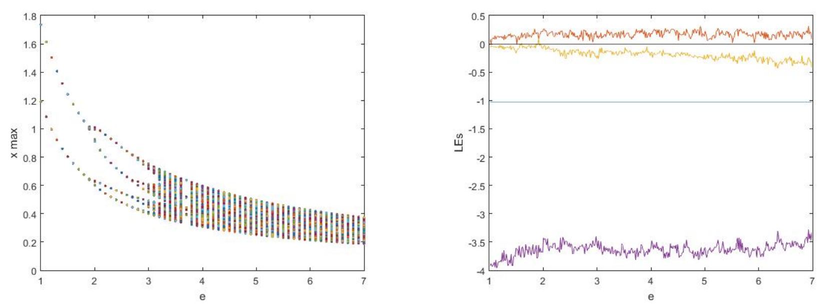

(A) (B)

FIGURE 9. Bifurcation of parameter $e \in [1, 7]$ at $c = 0.5$, $a = 0.1$, $b = 0.5$, $p = 4$, $d = 10$, and $\alpha = 0.98$ with initial conditions given by $(0, 5, 0, -0.1)$: **(a)** Bifurcation of e with xmax of system (3.3), **(b)** Bifurcation of e with LEs of system (3.3).

Fig. 10a describes the bifurcation of the system with parameter p, illustrating the system's evolving dynamics as parameter $p \in [1, 5]$. At values $(1.5 \leq p \leq 3)$, the system shows two clear branches of distinct points, corresponding to stable periodic states. As p increases $(3 < p < 3.8)$, the diagram displays period-doubling bifurcations, marked by a dense accumulation of points that signal the onset of chaotic behaviour. For $(p > 4)$, the chaos becomes more organized as p approaches 5. Bifurcation of Lyapunov spectrum with parameter p in Fig. 10b verifies the parameter p bifurcation with the system outcome. The diagram's clear transitions and point clustering effectively highlight the intricate balance between stability, period-doubling, and chaos, offering critical insights into the system's sensitivity to parameter variations p. We examined the system quasi-periodicity at $p = 3$ in Figs. 10c and 10d. while, the prevailed chaos in the system motion at $p = 4$ is depicted in Figs. 10e and 10f.

To examine how varying the parameter $\alpha \in [0, 1]$ impacts the system (3.3), bifurcation of parameter α with the system and the corresponding Lyapunov spectrum is shown in Figs. 11a and 11b, respectively. Through bifurcation analysis, it is evidenced that the fractional order α has a considerable influence on

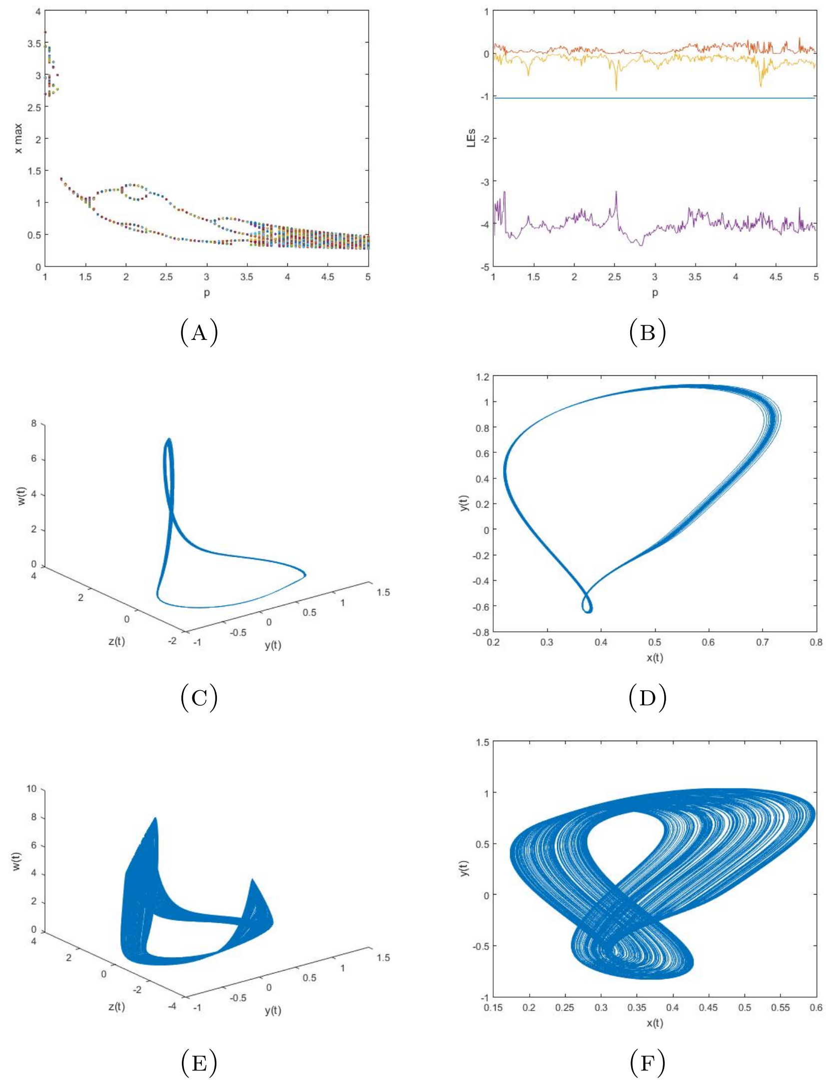

FIGURE 10. Bifurcation of parameter $p \in [1, 5]$ at $c = 0.5$, $e = 4$, $b = 0.5$, $a = 0.1$, $d = 10$, and $\alpha = 0.98$ with initial conditions given by $(0, 5, 0, -0.1)$: **(a)** Bifurcation of p with xmax of system (3.3), **(b)** Bifurcation of p with LEs of system (3.3), **(c)** Phase portrait at $p = 3$ in 3-D plane, **(d)** Phase portrait at $p = 3$ in $x - y$ plane, **(e)** Phase portrait at $p = 4$ in 3-D plane, **(f)** Phase portrait at $p = 4$ in $x - y$ plane.

the dynamic behaviour of the system, where it transits from unstable fixed points and periodic/quasi-periodic orbits ($0.8 \leq \alpha \leq 0.94$) to fully developed chaos as α approaches 1. In this way, this result affirms the critical role of fractional-order derivatives in determining the stability of the system; therefore, it increases the flexibility toward applications based on chaos. We illustrate the system behaviour at $\alpha = 0.88$ in Figs. 11c and 11d, while the investigation of the system quasi-periodic behaviour at $\alpha = 0.94$ is presented in Figs. 11e and 11f.

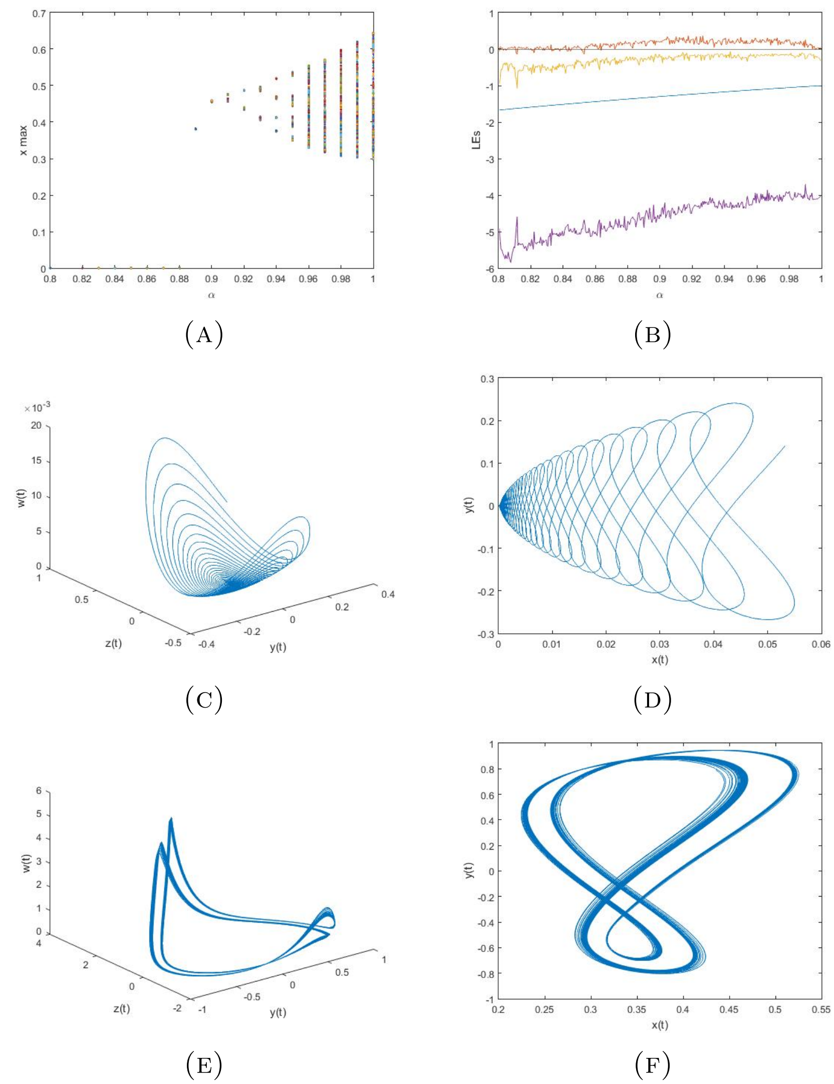

FIGURE 11. Bifurcation of parameter $\alpha \in [0.8, 1]$ at $a = 0.1$, $e = 4$, $b = 0.5$, $p = 4$, $c = 0.5$, and $d = 10$ with initial conditions given by $(0, 5, 0, -0.1)$: **(a)** Bifurcation of α with xmax of system (3.3), **(b)** Bifurcation of α with LEs of system (3.3), **(c)** Phase portrait at $\alpha = 0.88$ in 3-D plane, **(d)** Phase portrait at $\alpha = 0.88$ in $x - y$ plane, **(e)** Phase portrait at $\alpha = 0.94$ in 3-D plane, **(f)** Phase portrait at $\alpha = 0.94$ in $x - y$ plane.

4.5.2. *Effects of initial conditions.* In order to determine how sensitive the system is to the initial conditions, the parameters are selected as a, b, p, c, d, e, and α equal to 0.1, 0.5, 4, 0.5, 10, 4, and 0.98, respectively. Moreover, the spectrum of Lyapunov exponent and the system phase portraits are used.

To study the sensitivity of the initial condition $w(0)$, the other initial values are chosen as $x(0) = 0$, $y(0) = 5$, and $z(0) = 0$. The bifurcation of Lyapunov exponents with $w(0)$ diagram is shown in Fig. 12a, where the initial value $w(0)$ is varied from -15 to -5. It is evident that the initial value $w(0)$ determines the state of the suggested circuit. When $w(0)$ is between $[-15, -9.6]$, there exist periodic and quasi-periodic orbits, while when $w(0)$ is between $[-9.5, -5]$, a state of chaos is introduced into the system. The result emphasizes the strong dependence of the system's dynamics with respect to the initial condition $w(0)$, which thus plays a critical role in the transition between periodic, quasi-periodic, and chaotic behaviour for precision tuning in chaos-based applications. The system behaviour at initial conditions $[0, 5, 0, -15]$ and $[0, 5, 0, -5]$ is studied in Fig. 12b, where it is clear that the system at $w(0) = -5$ exists in an aperiodic state and the associated phase portraits are displayed in Figs. 12c, 12d and 12e, while at $w(0) = -15$ the system is in a quasi-periodic state and the related phase portraits are portrayed in Figs. 12f, 12g and 12h.

To examine the effect of $y(0)$ on the dynamics of the system, the other initial values are selected as $x(0) = 0$, $z(0) = 0$, and $w(0) = -0.1$. The Lyapunov exponents spectrum bifurcation with $y(0)$ portrait is shown in Fig. 13a, where the initial value $y(0)$ is increased from 2 to 7. It is clear to notice that the proposed circuit exhibits chaos when $y(0)$ is between $[2, 7]$. The study of the system behaviour at initial conditions $[0, 2, 0, -0.1]$ and $[0, 7, 0, -0.1]$ is reported in Fig. 13b. It is found that changing the value of $y(0) \in [2, 7]$ possesses an impact on the shape and pattern of the system strange attractors. When $y(0)$ is between $[2, 3.1]$ the system strange attractors have a shape inspected in Figs. 13c, 13d and 13e at $y(0) = 2$. In Figs. 13f, 13g and 13h at $y(0) = 3.5$, we can notice the start of the changing in the system strange attractors pattern. When $y(0)$ is between $[4, 7]$ the system strange attractors have another shape shown in Figs. 13i, 13j and 13k at $y(0) = 5$. This finding highlights the prominence of initial condition $y(0)$ in the chaotic dynamics of the proposed system where basically changes in the control parameter $y(0)$ do sustain the chaos but change the structure of strange attractors; hence, its consideration becomes important in terms of control or optimization of chaotic behaviour in practical applications.

4.6. **Numerical simulation.** For a, b, c, d, and e, holding the values 0.1, 0.5, 0.5, 10, and 4, respectively, the numerical simulation of the proposed system (3.3) using Adams-Bashforth-Moulton algorithm is shown in Fig. 14 at $p = 4$ and $\alpha = 0.98$, where it is clear that the trajectories are aperiodic, unpredictable, and change in a constrained complex manner. These aspects give basic explanations of chaos and strange attractors. In Fig. 15 at $p = 4$ and $\alpha = 1$, it is easily perceived that the system also exhibits chaotic motion in the integer case, which confirms the obtained result from α bifurcation.

5. Circuit design and experiment results

The accepted definition of a fractional calculus does not permit the straightforward execution of fractional operators within the domain simulations, hindering the analysis of fractional-order systems. However, based on the concepts of circuit

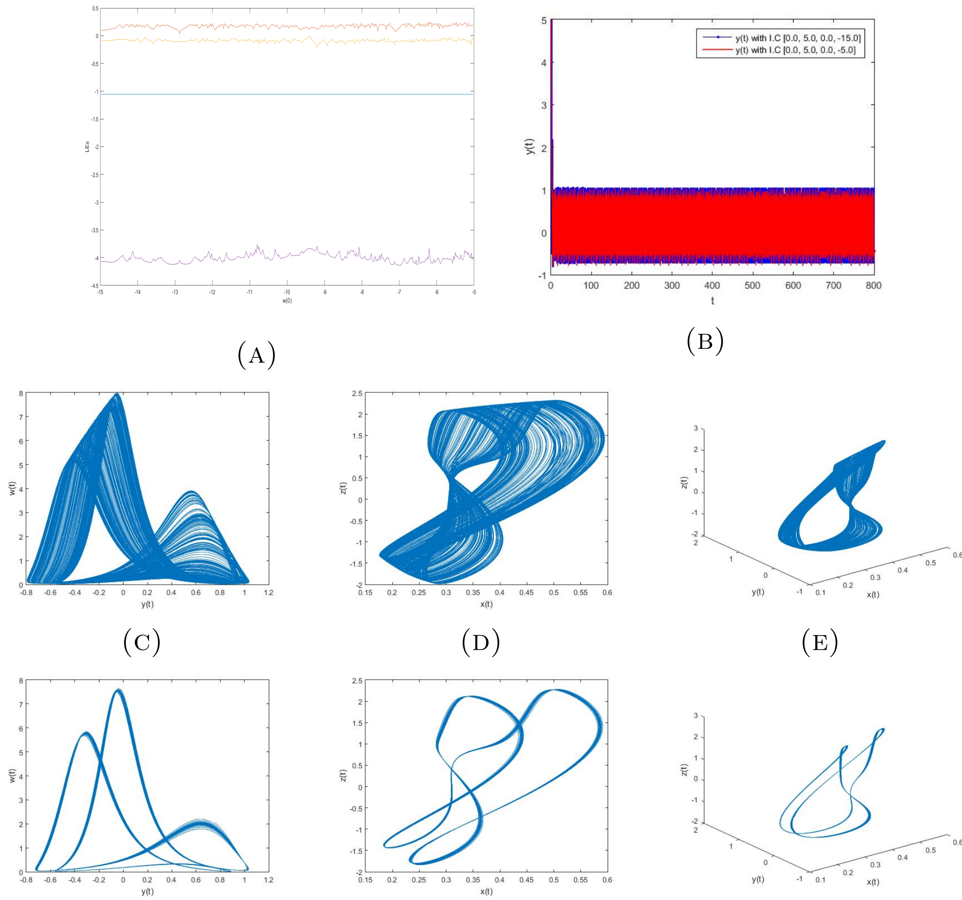

(A) (B)

(C) (D) (E)

(F) (G) (H)

FIGURE 12. The influence of changing $w(0)$ from -15 to -5: **(a)** Bifurcation of $w(0)$ with LEs of system (3.3), **(b)** Comparison of system (3.3) behaviour with two different values of $w(0)$, **(c)** $y-w$ plane at $w(0)=-5$, **(d)** $x-z$ plane at $w(0)=-5$, **(e)** 3-D plane at $w(0)=-5$, **(f)** $y-w$ plane at $w(0)=-15$, **(g)** $x-z$ plane at $w(0)=-15$, **(h)** 3-D plane at $w(0)=-15$.

theory, the fractional-order integrator can be linearly approximated to its integer order approximation, utilizing frequency domain techniques derived from Bode plots. To rationalize the fractional order components, various iterative strategies can be used, as described in [58, 23]. The approach used in this research is Charef's method [19] which is the most popular technique because it achieves an excellent balance between complexity and approximate accuracy. The approximation formula of $\frac{1}{s^{\alpha}}$ where $\alpha = 0.98$, as introduced in [34], is given by

$$\frac{1}{s^{0.98}} = \frac{1.2974\,(s+1125)}{(s+1423)\,(s+0.01125)}\,, \tag{5.1}$$

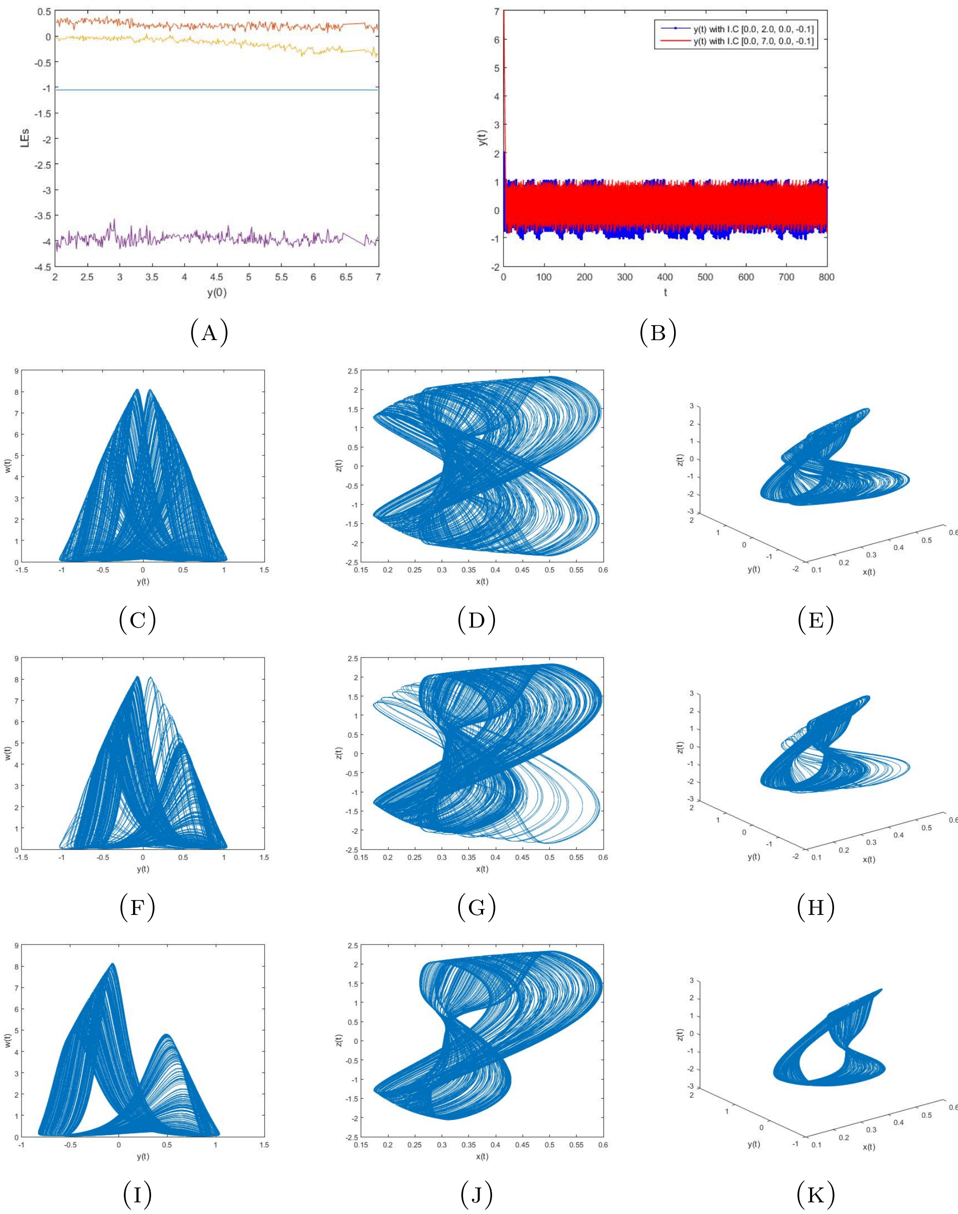

FIGURE 13. The influence of changing $y(0)$ from 2 to 7: **(a)** Bifurcation of $y(0)$ with LEs of system (3.3), **(b)** Comparison of system (3.3) behaviour with two different values of $y(0)$, **(c)** $y - w$ plane at $y(0) = 2$, **(d)** $x - z$ plane at $y(0) = 2$, **(e)** 3-D plane at $y(0) = 2$, **(f)** $y - w$ plane at $y(0) = 3.5$, **(g)** $x - z$ plane at $y(0) = 3.5$, **(h)** 3-D plane at $y(0) = 3.5$, **(i)** $y - w$ plane at $y(0) = 5$, **(j)** $x - z$ plane at $y(0) = 5$, **(k)** 3-D plane at $y(0) = 5$

where $s = jw$. The chain ship circuit component shown in Fig. 16 which simulates the behaviour of the fractional integral operator has a transfer function between the connecting nodes A and B as shown below

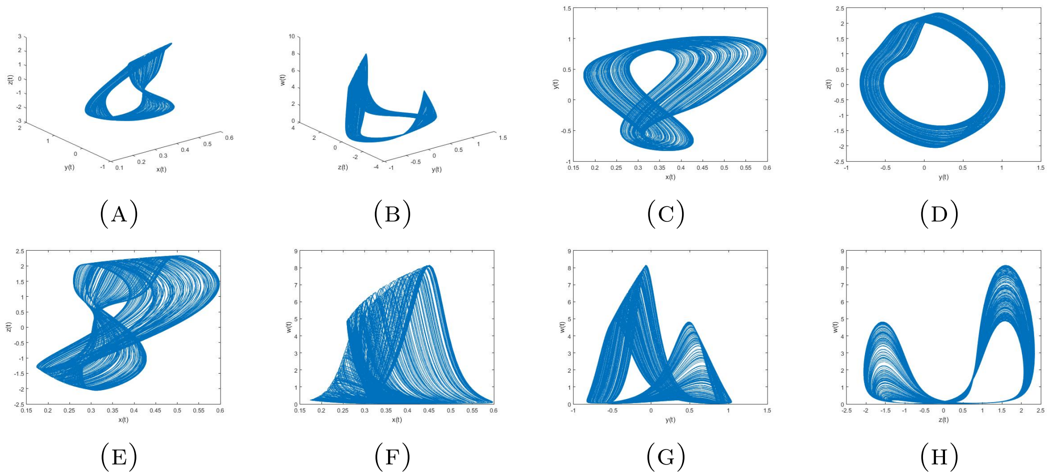

FIGURE 14. 3-D and 2-D numerical simulation of the proposed system (3.3) at $\alpha = 0.98$ and $p = 4$ with initial conditions $(0, 5, 0, -0.1)$.

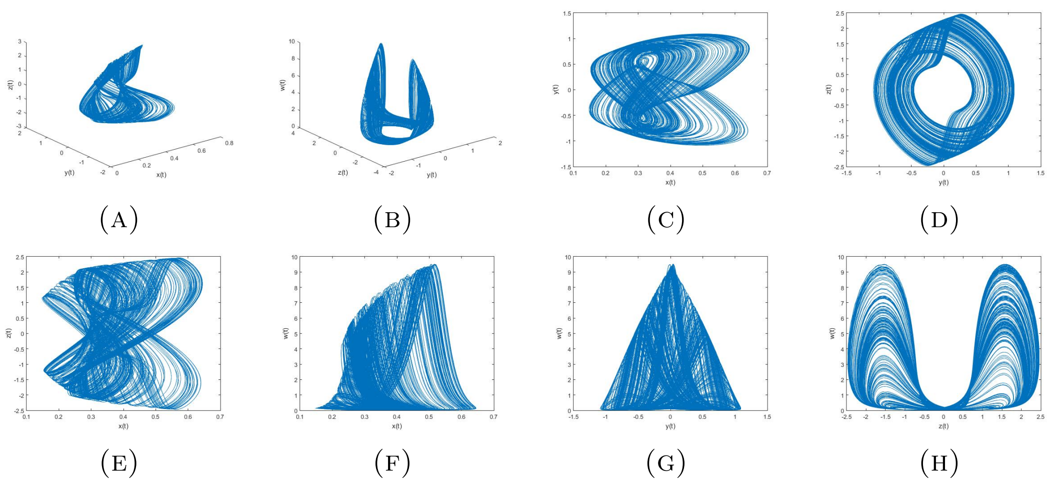

FIGURE 15. 3-D and 2-D numerical simulation of the proposed system (3.3) at $\alpha = 1$ and $p = 4$ with initial conditions $(0, 5, 0, -0.1)$.

$$H_{0.98}(s) = \frac{R_1}{sR_1C_1 + 1} + \frac{R_2}{sR_2C_2 + 1} \tag{5.2}$$

$$= \frac{1}{C_0} \frac{\left(\dfrac{C_0}{C_1} + \dfrac{C_0}{C_2}\right)\left[s + \dfrac{\frac{1}{R_1} + \frac{1}{R_2}}{C_1 + C_2}\right]}{\left(s + \dfrac{1}{R_1C_1}\right)\left(s + \dfrac{1}{R_2C_2}\right)}, \tag{5.3}$$

taking $C_0 = 1\ \nu$F. Since $H(s)\,C_0 = \dfrac{1}{s^{0.98}}$, we can get $R_1 = 190.933\,\Omega$, $R_2 = 91.1873\,M\Omega$, $C_1 = 3.68059\,\mu F$ and $C_2 = 975.32\,nF$.

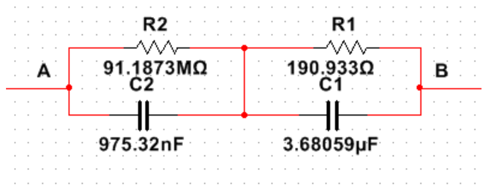

FIGURE 16. The chain ship unit of $\frac{1}{s^{0.98}}$ [34].

Based on the previous analysis, the system given by equation (3.3) indicates that a chaotic state is present in the system when the parameters a, b, p, c, d, e, and α, are defined as 0.1, 0.5, 4, 0.5, 10, 4, and 0.98, respectively. The experimental circuit that has been designed is illustrated in Fig. 17, and this circuit can be characterized by

$$\begin{aligned}
{}_0^cD_\tau^\alpha x &= \left(\frac{R_{10}}{R_{34}}\right) y^2 - \left(\frac{R_{10}}{R_{12}}\right) x,\\
{}_0^cD_\tau^\alpha y &= -\left(\frac{R_{21}}{R_{22}}\right) z,\\
{}_0^cD_\tau^\alpha z &= -\left(\frac{R_{26}}{R_{32}}\right) zw^2 + \left(\frac{R_{26}}{R_{27}}\right) z + \left(\frac{R_{26}}{R_{13}}\right) y,\\
{}_0^cD_\tau^\alpha w &= \left(\frac{R_{15}}{R_{11}}\right) z - \left(\frac{R_{15}}{R_{16}}\right) w + \left(\frac{R_{15}}{R_{17}}\right) z^2 w,
\end{aligned} \tag{5.4}$$

where the values of all resistors are illustrated in Fig. 17. The experimental simulation of the oscilloscopes reported in Fig. 18 shows the same chaotic behaviour obtained from the numerical simulation.

6. SOUND ENCRYPTION

Recently, chaos-based cryptography has gained popularity due to its desired characteristics, such as: complexity, sensitivity to parameter changes, and pseudo-randomness. Chaos-based cryptography uses concepts of chaos theory to mask and unmask the data. The application of chaos theory in encryption makes cryptography extremely secure due to the unpredictable nature of chaos theory and one-time pad cryptography as in this method we use a unique key for each message quickly and efficiently. Examples of chaotic systems or chaotic maps, often called pseudo-random number generators (PRNGs), used in cryptography applications are described in [39, 15, 28, 18, 36, 35].

Thus, in this section, a PRNG is implemented to encrypt a sound signal using the proposed system in (3.3). NIST-800-22 randomness tests [54] were performed on the pseudorandom numbers produced by the proposed chaotic system; Table 2 displays the test's successful results. The generated keystream based on the proposed system in (3.3) is dependent on the original sound data in addition to the fractional system parameters and initial conditions.

6.1. Encryption technique.

This subsection provides the steps of the encryption technique based on (3.3) as follows

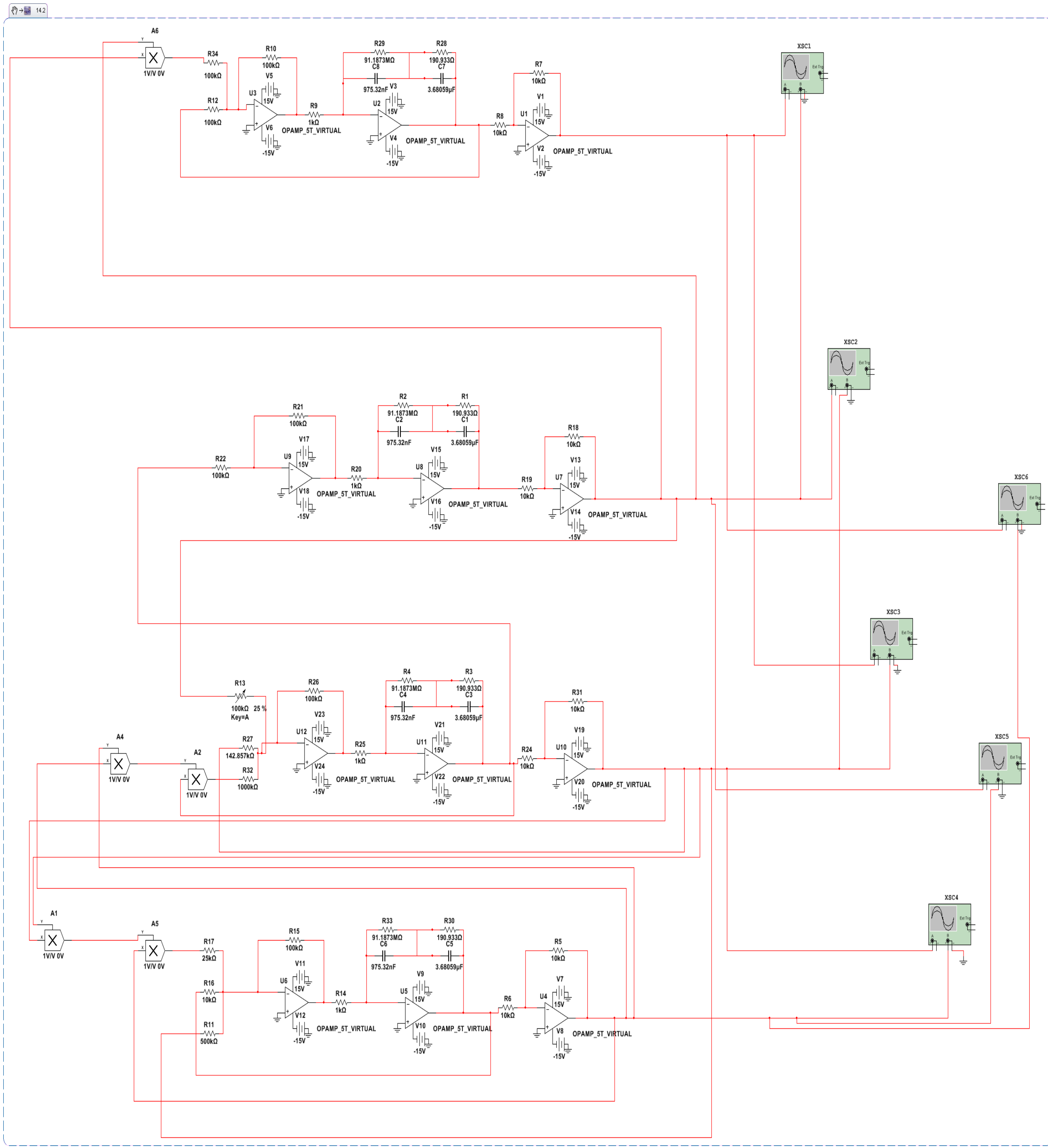

FIGURE 17. The implementation of the proposed circuit at $\alpha = 0.98$.

- Read the sound signal into matlab where it is stored as a $n \times 2$ matrix: $S = [\overrightarrow{m}\,\overrightarrow{r}]$.
- Shuffle the matrix $S_{n\times 2}$ by row using an index of random unrepeated integers.

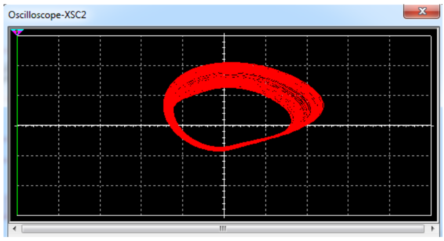

(A)

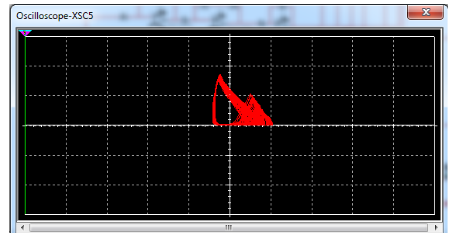

(B)

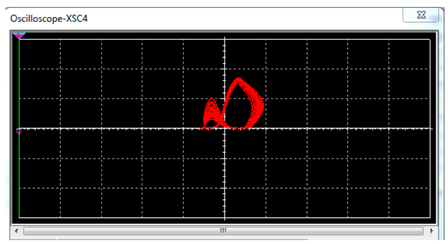

(C)

FIGURE 18. Experimental simulation of the proposed circuit at $\alpha = 0.98$ and $p = 4$: **(a)** Oscilloscope observation of the proposed system's attractors in chaos in the $y-z$ plane, **(b)** Oscilloscope observation of the proposed system's attractors in chaos in the $y-w$ plane, **(c)** Oscilloscope observation of the proposed system's attractors in chaos in the $z-w$ plane.

- Determine the perturbation value H_{aud}, which is a constant parameter relies only on the original sound signal and is evaluated by
$$H_{aud} = \left(\sum_{t=1}^{n} S(t,1) + \sum_{t=1}^{n} S(t,2) \right) \Big/ (n \times 2). \tag{6.1}$$
- Add H_{aud} to the system parameter p or to the initial conditions and skip the first transient values to get a time series solution as $x(k)$, $y(k)$, $z(k)$, and $w(k)$ where $k = 1, 2, 3, ..., n$ and x, y, z, w are regarded as the state variables of the system. Choose any two state variables of them as a secret key K_s.
- Add the secret key K_s to the shuffled matrix $S_{n\times 2}$ to get the encrypted sound signal.

Reverse the encryption steps to perform decryption as outlined below

- Read the encrypted sound signal as a matrix $n \times 2$, then subtract the secret key K_s from it.
- Deshuffle the obtained matrix by row using the same previous generated index to get the decrypted sound signal.

Fig. 19 displays the block diagram that depicts encryption/decryption process. The proposed algorithm is applied to a float sound signal shown in Fig. 20, where Fig. 20a represents the original sound spectrum, Fig. 20b represents the encrypted sound spectrum where it is noticeable that the spectrum is completely

TABLE 2. Results of NIST statistical test [54] carried out on the pseudorandom numbers generated from the proposed system.

Test Name	x (P-value)	y (P-value)	z (P-value)	w (P-value)	Status
1. Frequency (Monobit) Test	0.2444	0.2201	0.7009	0.5578	Passed
2. Frequency Test within a Block	0.7737	0.0820	0.1500	0.3261	Passed
3. Runs Test	0.9462	0.6777	0.8242	0.8295	Passed
4. Test for the Longest Run of Ones in a Block	0.4845	0.1754	0.36165	0.6953	Passed
5. Binary Matrix Rank Test	0.2236	0.3050	0.3247	0.2625	Passed
6. Non-overlapping Template Matching Test	0.5614	0.0385	0.7795	0.5219	Passed
7. Overlapping Template Matching Test	0.4637	0.9398	0.1490	0.2745	Passed
8. Maurer's "Universal Statistical" Test	0.3495	0.2109	0.2902	0.2895	Passed
9. Linear Complexity Test	0.0186	0.6708	0.3951	0.7133	Passed
10. Serial Test					
P-value 1:	0.5068	0.4332	0.7923	0.3487	
					Passed
P-value 2:	0.9489	0.6803	0.5727	0.1841	
11. Approximate Entropy Test	0.2900	0.1965	0.3425	0.6039	Passed
12. Cumulative Sums (Cusum) Test					
P-value Forward:	0.2318	0.3545	0.7728	0.6164	
					Passed
P-value Reverse:	0.6037	0.5729	0.9433	0.2191	
13. Random Excursions Test	0.0147	0.1568	0.0111	0.4176	Passed
14. Random Excursions Variant Test	0.0125	0.0180	0.2417	0.0199	Passed

changed and original data cannot be recognized. Fig. 20c shows the decoded sound spectrum, it is obvious that the spectrum of the original sound and the decoded sound are identical.

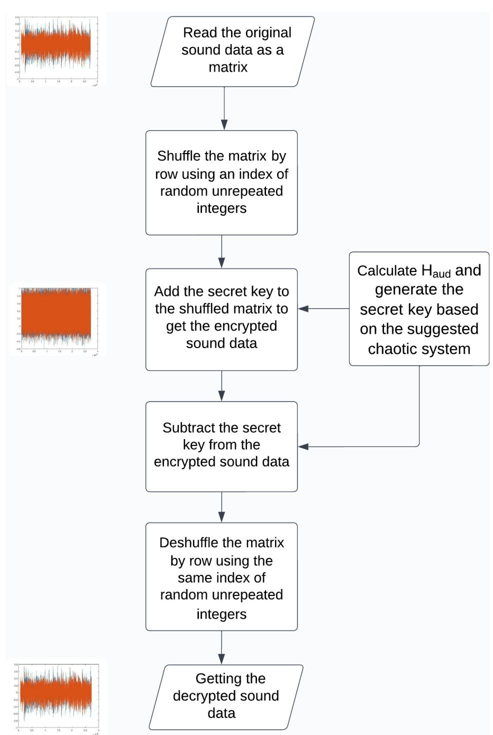

FIGURE 19. Encryption and decryption process block diagram.

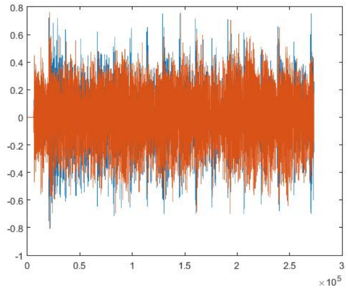

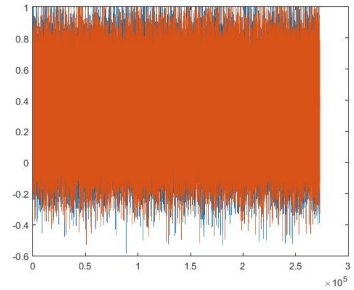

(A) The original sound signal. (B) The encrypted sound signal.

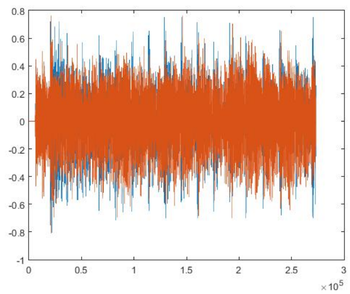

(C) The decrypted sound signal.

FIGURE 20. The encrypted and decrypted sound signal spectrum.

6.2. **Encryption performance and comparative analysis.** Table 3 shows the comparison between the sound encryption algorithm based on the novel memristive chaotic circuit proposed in this research and The Advanced Encryption Standard (AES) [52]. In contrast with traditional audiovisual AES encryption that is built around the concept of key expansion and utilizes block ciphering, the new memristive chaos-based encryption scheme is superior by randomness, differential attack resistance, as well as key sensitivity. Traditional encryption approaches, such as AES, are implemented in a block and type format that has a fixed-length, and therefore requires substantial computational resources, which makes the instantaneous encryption of high frequency sound signals almost impossible [24]. Hence, the new approach has the ability to increase security and efficiency at the same time. Unlike the existing methods, this approach is more flexible and can be used in real-time and limited resource settings, thus making it more appealing than standard cryptography methods.

It is necessary to analyse and verify the encoding and decoding durations of various algorithms in order to assess their efficacy. This helps to determine which algorithms aim to offer better performance and more security. Table 4 defines two different algorithms encoding and decoding times and the speed at which these processes are done. It is clear that rapid speed criteria are successfully fulfilled for both the encryption and decryption procedures based on the proposed (PRNG).

Complex and extremely unpredictable dynamics characterise the suggested fractional-order chaotic circuit with a feedback memristor, which makes it a viable option for a variety of cutting-edge engineering and security applications.

Table 3. Comparison between AES and Chaos-based Encryption for sound signals.

Feature	AES-Based Encryption	Chaos-based Encryption
Key Sensitivity	Low	High
	(Small key changes barely impact encryption output)	(Minor changes in conditions cause drastically different outputs)
Computational Complexity	High	Low
	(substitution-permutation on network, key expansion)	(relies on simple chaotic iteration)
Real-Time Suitability	Limited	High
	(block-wise encryption introduces latency)	(continuous chaotic perturbation enables real time processing)
Resistance to Differential Attacks	Moderate	High
	(dependent on S-box and diffusion mechanism)	(chaotic systems naturally amplify small differences)
Vulnerability to Side-Channel Attacks	Moderate to High	Low
	(power analysis can reveal cryptographic operations)	(chaotic dynamics obscure key-related computations)
Implementation on Low-Power Devices	Computationally expensive	Energy-efficient due to lightweight chaotic operations

Table 4. Time comparison between AES and Chaos-based Encryption for sound signals.

	Chaos-based Encryption This paper	AES-based Encryption (Matlab) [60]
Encryption Time	12.979 ms	15.510 ms
Decryption time	13.864 ms	14.185 ms

Beyond its proven success in sound encryption, these chaotic circuits have been extensively investigated for secure communication systems, where their sensitivity to initial conditions strengthens encryption schemes' resistance to differential cryptanalysis and brute-force attacks [48]. Chaotic systems can be applied in signal processing for random number generation, noise suppression, and spread-spectrum communication – all of which contribute towards efficient modern cryptographic systems [64]. Moving the focus from neural networks to deep learning models, some recent research exploits the concept of chaos to enhance learning efficiency and help deep learning models overcome the challenge of local minimum [46]. Given these diverse applications, the proposed chaotic circuit merits further investigation in the fields of cybersecurity frameworks, next-generation artificial intelligence models, and biological signal encryption.

7. Conclusion

A new fractional-order chaotic circuit featuring an integrated feedback memristor is introduced in this work. The mathematical model and circuit fractional-order design are created and studied. Numerical simulations and stability analysis are used to illustrate the chaotic nature of the system and the existence of coexisting attractors. The complex nonlinear dynamics of the proposed circuit, including periodic, quasi-periodic, and chaotic behaviours, are investigated and illustrated. Strong agreement between the theoretical results and the numerical analysis is demonstrated by the carried out experimental simulations. Furthermore, the chaotic sequences produced by the proposed fractional-order memristive system successfully pass the NIST 800-22 randomness tests, demonstrating its potential for secure encryption. These sequences provide a stable and fast sound encoding system that ensures a completely transformed sound spectrum without any recognizable original data.

Conflict of interest The authors declare that they have no conflict of interest.

Acknowledgement. The author(s) would like to express their sincere appreciation to the editorial board and reviewers of Gulf Journal of Mathematics for their valuable time, insightful comments, and constructive feedback, which have significantly contributed to improving the quality of this work.

References

1. Abbes, A., Ouannas, A., Hioual, A., & Momani, S. (2024). Hidden Chaos in a new memristor-based discrete system with commensurate, incommensurate and variable fractional orders. Physica Scripta, 99(10), 105233. equations, 2021, 1-24. https://doi.org/10.1088/1402-4896/ad7361
2. Aburakhis, M., & *Ordóñez*, R. (2024). Generalization of Direct Adaptive Control Using Fractional Calculus Applied to Nonlinear Systems. Journal of Control, Automation and Electrical Systems, 35(3), 428-439. https://doi.org/10.1007/s40313-024-01082-0
3. AGUILAR, J. F. G. (2016). Behavior characteristics of a cap-resistor, memcapacitor, and a memristor from the response obtained of RC and RL electrical circuits described by fractional differential equations. Turkish Journal of Electrical Engineering and Computer Sciences, 24(3). https://doi.org/10.3906/elk-1312-49
4. Aguirre, F., Sebastian, A., Le Gallo, M., Song, W., Wang, T., Yang, J. J., ... & Lanza, M. (2024). Hardware implementation of memristor-based artificial neural networks. Nature communications, 15(1), 1974. https://doi.org/10.1038/s41467-024-45670-9
5. Ahmed, E., El-Sayed, A. M. A., & El-Saka, H. A. (2006). On some Routh–Hurwitz conditions for fractional order differential equations and their applications in Lorenz, *Rössler*, Chua and Chen systems. Physics Letters A, 358(1), 1-4. https://doi.org/10.1016/j.physleta.2006.04.087
6. Allagui, A., Freeborn, T. J., Elwakil, A. S., Fouda, M. E., Maundy, B. J., Radwan, A. G., ... & Abdelkareem, M. A. (2018). Review of fractional-order electrical characterization of supercapacitors. Journal of Power Sources, 400, 457-467. https://doi.org/10.3906/elk-1312-49
7. Alzahrani, A. B., Saadeh, R., Abdoon, M. A., Elbadri, M., Berir, M., & Qazza, A. (2024). Effective methods for numerical analysis of the simplest chaotic circuit model with atangana–baleanu caputo fractional derivative. Journal of Engineering Mathematics, 144(1), 9. https://doi.org/10.1007/s10665-023-10319-x
8. Babrhou, Y., Cherkaoui, F., El Boukari, B., Hilal, K., & Kajouni, A. (2025). Analysis and optimal control of a fractional-order SEAIR epidemic model with two-strains. Gulf Journal of Mathematics, 19(1), 251-284. https://doi.org/10.56947/gjom.v19i1.2561
9. Bao, B., Ma, Z., Xu, J., Liu, Z., & Xu, Q. (2011). A simple memristor chaotic circuit with complex dynamics. International Journal of Bifurcation and Chaos, 21(09), 2629-2645. https://doi.org/10.1142/S0218127411029999
10. Bao, B., Shi, G., Xu, J., Liu, Z., & Pan, S. (2011). Dynamics analysis of chaotic circuit with two memristors. Science China Technological Sciences, 54, 2180-2187. https://doi.org/10.1007/s11431-011-4400-6
11. Barbero, G., Evangelista, L. R., Zola, R. S., Lenzi, E. K., & Scarfone, A. M. (2024). A brief review of fractional calculus as a Tool for Applications in Physics: Adsorption

Phenomena and Electrical Impedance in Complex Fluids. Fractal and Fractional, 8(7), 369. https://doi.org/10.3390/fractalfract8070369

12. Barraj, I., Mestiri, H., & Masmoudi, M. (2024). Overview of Memristor-Based Design for Analog Applications. Micromachines, 15(4), 505. https://doi.org/10.3390/mi15040505
13. Batas, D., & Fiedler, H. (2010). A memristor SPICE implementation and a new approach for magnetic flux-controlled memristor modeling. IEEE Transactions on Nanotechnology, 10(2), 250-255. https://doi.org/10.1109/TNANO.2009.2038051
14. Benderli, S., & Wey, T. A. (2009). On SPICE macromodelling of TiO^ sub C^ memristors. Electronics letters, 45(7), 1. https://doi.org/10.1049/el.2009.3511
15. Benkouider, K., Sambas, A., Bonny, T., Al Nassan, W., Moghrabi, I. A., Sulaiman, I. M., ... & Mamat, M. (2024). A comprehensive study of the novel 4D hyperchaotic system with self-exited multistability and application in the voice encryption. Scientific Reports, 14(1), 12993. https://doi.org/10.1038/s41598-024-63779-1
16. Butzer, P. L., & Westphal, U. (2000). An introduction to fractional calculus. In Applications of fractional calculus in physics (pp. 1-85). https://doi.org/10.1142/9789812817747_0001
17. Campbell, K. A. (2017). Self-directed channel memristor for high temperature operation. Microelectronics journal, 59, 10-14. https://doi.org/10.1016/j.mejo.2016.11.006
18. Cao, G., Tao, Y., Liu, X., & Zhang, T. (2024). Image encryption based on a coined chaotic system and high-intensity encryption primitives. IEEE access. http://doi.org/10.1109/ACCESS.2024.3423691
19. Charef, A., Sun, H. H., Tsao, Y. Y., & Onaral, B. (1992). Fractal system as represented by singularity function. IEEE Transactions on automatic Control, 37(9), 1465-1470. https://doi.org/10.1109/9.159595
20. Chua, L. (1971). Memristor-the missing circuit element. IEEE Transactions on circuit theory, 18(5), 507-519 https://doi.org/10.1088/0268-1242/29/10/104001
21. Chua, L. (2014). If it's pinched it'sa memristor. Semiconductor Science and Technology, 29(10), 104001. https://doi.org/10.1088/0268-1242/29/10/104001
22. Chua, L. O., & Kang, S. M. (1976). Memristive devices and systems. Proceedings of the IEEE, 64(2), 209-223. https://doi.org/10.1109/PROC.1976.10092
23. *Colín-Cervantes, J. D., Sánchez-López, C., Ochoa-Montiel, R., Torres-Muñoz, D., Hernández-Mejía, C. M., Sánchez-Gaspariano, L. A., & González-Hernández, H. G. (2021). Rational approximations of arbitrary order: A survey. Fractal and Fractional, 5(4), 267.* https://doi.org/10.3390/fractalfract5040267
24. Daemen, J., & Rijmen, V. (2002). The design of Rijndael. (Vol. 2). New York: Springer-verlag.
25. Daimary, N., & Paul, R. (2024). Analysis of a fractional-order mathematical model for occupational transition from farming to other sectors. Gulf Journal of Mathematics, 18(1), 165-188. https://doi.org/10.56947/gjom.v18i1.2196
26. Danca, M. F., & Kuznetsov, N. (2018). Matlab code for Lyapunov exponents of fractional-order systems. International Journal of Bifurcation and Chaos, 28(05), 1850067. https://doi.org/10.1142/S0218127418500670
27. Daoui, A., Yamni, M., Pławiak, P., Alfarraj, O., & Abd El-Latif, A. A. (2024). A New Chaotic Memristor-Based Cryptosystem for Secure Bio-Signal Transmission on Low-Cost Hardware. IEEE Access. https://doi.org/10.1109/ACCESS.2024.3408136
28. Darani, A. Y., Yengejeh, Y. K., Pakmanesh, H., & Navarro, G. (2024). Image encryption algorithm based on a new 3D chaotic system using cellular automata. Chaos, Solitons & Fractals, 179, 114396. https://doi.org/10.1016/j.chaos.2023.114396
29. Deressa, C. T., Etemad, S., & Rezapour, S. (2021). On a new four-dimensional model of memristor-based chaotic circuit in the context of nonsingular *Atangana–Baleanu–Caputo* operators. Advances in difference equations, 2021, 1-24. https://doi.org/10.1186/s13662-021-03600-9

30. Ferrari, A. L., Gomes, M. C. S., Aranha, A. C. R., Paschoal, S. M., de Souza Matias, G., de Matos Jorge, L. M., & Defendi, R. O. (2024). Mathematical modeling by fractional calculus applied to separation processes Separation and Purification Technology, 337, 126310. https://doi.org/10.1016/j.seppur.2024.126310
31. Ganie, A. H., Aljuaydi, F., Ahmad, Z., Bonyah, E., Khan, N., Alharthi, N. S., ... & AlBaidani, M. M. (2024). A fractal–fractional perspective on chaotic behavior in 4D memristor-nonlinear system. AIP Advances, 14(1). https://doi.org/10.1063/5.0187218
32. Geraghty, P. (2024). Modeling a financial system with memory via fractional calculus and fractional Brownian motion. *arXiv preprint arXiv*:2406.19408. https://arxiv.org/abs/2406.19408
33. Gokyildirim, A., Calgan, H. & Demirtas, M. (2024). Fractional-Order sliding mode control of a 4D memristive chaotic system. Journal of Vibration and Control, 30(7-8), 1604-1620. https://doi.org/10.1177/10775463231166187
34. Hammouch, Z., & Mekkaoui, T. (2018). Circuit design and simulation for the fractional-order chaotic behavior in a new dynamical system. Complex & Intelligent Systems, 4(4), 251-260. https://doi.org/10.1007/s40747-018-0070-3
35. Haridas, T., Upasana, S. D., Vyshnavi, G., Krishnan, M. S., & Muni, S. S. (2024). Chaos-based audio encryption: Efficacy of 2D and 3D hyperchaotic systems. Franklin Open, 8, 100158. https://doi.org/10.1016/j.fraope.2024.100158
36. Haseeb, E. H., Kadhim, S. A., & Mahmood, A. S. (2023). A Six-Dimensional Hyperchaotic Pseudorandom Sequence for Enhanced Voice Encryption. *Ingénierie des Systèmes d'Information*, 28(4). https://doi.org/10.18280/isi.280425
37. Hattaf, K. (2024) A new mixed fractional derivative with applications in computational biology. Computation, 12(1), 7. https://doi.org/10.20944/preprints202311.0242.v1
38. Jesus, I. S., & Tenreiro Machado, J. A. (2009). Development of fractional order capacitors based on electrolyte processes. Nonlinear Dynamics, 56, 45-55. https://doi.org/10.1007/s11071-008-9377-8
39. Kamal, F. M., Elsonbaty, A., & Elsaid, A. (2021). A novel fractional nonautonomous chaotic circuit model and its application to image encryption. Chaos, Solitons & Fractals, 144, 110686. https://doi.org/10.1016/j.chaos.2021.110686
40. Kamdem, T. C., Richard, K. G., & *Béda*, T. (2024). Modeling the mechanical behavior of rock during plastic flow using fractional calculus theory. Applied Mathematical Modelling. https://doi.org/10.1016/j.apm.2024.03.025
41. Kausar, A., Chang, C. Y., Raja, M. A. Z., & Shoaib, M. (2025). A novel design of layered recurrent neural networks for fractional order *Caputo–Fabrizio* stiff electric circuit models. Modern Physics Letters B, 39(02), 2450393. https://doi.org/10.1142/S0217984924503937
42. Miller, K. S. (1993). An introduction to the fractional calculus and fractional differential equations. John Willey & Sons.
43. Mostafa, S., Amer, F. Z., ElKhatib, M. M., & Mubarak, R. I. (2024). Memristors Modelling and Simulation for Digital to Analog Converter Circuit. Russian Microelectronics, 53(2), 188-195. https://doi.org/10.1134/S1063739723600723
44. Mu, P., Wang, L., & Liu, C. (2020). A control parameterization method to solve the fractional-order optimal control problem. Journal of Optimization Theory and Applications, 187(1), 234-247. https://doi.org/10.1007/s10957-017-1163-7
45. Parajuli, S., Budhathoki, R. K., & Kim, H. (1905). Nonvolatile memory cell based on memristor emulator (2019). *Preprint arXiv*. https://doi.org/10.48550/arXiv.1905.04864
46. Pathak, J., Hunt, B., Girvan, M., Lu, Z., & Ott, E. (2018). Model-free prediction of large spatiotemporally chaotic systems from data: A reservoir computing approach. *Physical review letters*, 120(2), 024102. https://doi.org/10.1103/PhysRevLett.120.024102
47. *Petráš* I. (2008). A note on the fractional-order Chua's system. Chaos, Solitons & Fractals, 38(1), 140-147. https://doi.org/10.1016/j.chaos.2006.10.054

48. Pisarchik, A. N., & Zanin, M. (2010). Chaotic map cryptography and security. Encryption: Methods, Software and Security, 1-28.
49. Podlubny, I. (1999). An introduction to fractional derivatives, fractional differential equations, to methods of their solution and some of their applications. *Math. Sci. Eng*, 198(340), 0924-34008.
50. Raorane, A. A., Patil, M. D., & Vyawahare, V. A. (2015, May). Analysis of full-wave controlled rectifier with lossy inductive load using fractional-order models. In 2015 International Conference on Industrial Instrumentation and Control (ICIC) (pp. 750-755). IEEE. https://doi.org/10.1109/IIC.2015.7150842
51. Rayal, A., Anand, M., & Srivastava, V. K. (2024). Application of fractional modified taylor wavelets in the dynamical analysis of fractional electrical circuits under generalized caputo fractional derivative. *Physica Scripta*, 99(12), 125255. http://doi.org/10.1088/1402-4896/ad8701
52. Rijmen, V., & Daemen, J. (2001). Advanced encryption standard. Proceedings of federal information processing standards publications, national institute of standards and technology, 19, 22.
53. *Robles, E. H., Torres, F. J., Balvantín-García, A. J., Martínez-Ramírez, I., Capilla, G., & Ramírez-Paredes, J. P. (2024). Fractional Calculus Applied to the Generalized Model and Control of an Electrohydraulic System. Fractal and Fractional*, 8(12), 679. https://doi.org/10.3390/fractalfract8120679
54. Rukhin, A. (2001). A statistical test suite for random and pseudorandom number generators for cryptographic applications. *Booz-Allen and Hamilton Inc Mclean Va.*
55. Sabarathinam, S., Aravinthan, D., Papov, V., Vadivel, R., & Gunasekaran, N. (2024). Least fractional order memristor nonlinearity to exhibits chaos in a hidden hyperchaotic system. *Fractional Calculus and Applied Analysis*, 27(5), 2502-2520. https://doi.org/10.1007/s13540-024-00319-8
56. Sadek, L. (2024). Control theory for fractional differential Sylvester matrix equations with Caputo fractional derivative. *Journal of Vibration and Control*, 10775463241246430. https://doi.org/10.1177/10775463241246430
57. Selvam, A. P., & Govindaraj, V. (2024). Investigation of controllability and stability of fractional dynamical systems with delay in control. *Mathematics and Computers in Simulation*, 220, 89-104. https://doi.org/10.1016/j.matcom.2024.01.011
58. Serrano, E. Z. (2017). Fractional order chaotic systems and their electronic design. *Instituto Potosino de Investigation cientifica y tecnologica, AC.*
59. Shafiq, M., & Ahmad, I. (2024). Chatter-Free Adaptive Control of a Memristor-Based Four-Dimensional Chaotic Oscillator. *Arabian Journal for Science and Engineering*, 7677-7699. https://doi.org/10.1007/s13369-023-08587-x
60. Shah, B., & Aalam, Z. Implementation and Performance Evaluation of the AES Algorithm for Data Transmission using Various Programming Languages. *Communications on Applied Electronics (CAE)–ISSN*, 2394-4714. http://doi.org/10.5120/cae2015651928
61. Song, F., Shao, H., Ming, J., Sun, J., Li, W., Yi, M., ... & Ling, H. (2024). Dynamic Memristors for Temporal Signal Processing. *Advanced Materials Technologies*, 9(16), 2400764. https://doi.org/10.1002/admt.202400764
62. Strogatz, S. H. (2018). Nonlinear dynamics and chaos with student solutions manual: With applications to physics, biology, chemistry, and engineering. CRC press.
63. Strukov, D. B., Snider, G. S., Stewart, D. R., & Williams, R. S. (2008). The missing memristor found. *nature*, 453(7191), 80-83. https://doi.org/10.1038/nature06932
64. Suykens, J. A., Vandewalle, J. P., & De Moor, B. L. (2012). Artificial neural networks for modelling and control of non-linear systems. Springer Science & Business Media.
65. Tetzlaff, R., & Schmidt, T. (2012, May). Memristors and memristive circuits-an overview. In 2012 IEEE International Symposium on Circuits and Systems (ISCAS) (pp. 1590-1595). IEEE. https://doi.org/10.1109/ISCAS.2012.6271557

66. Tlelo-Cuautle, E., Pano-Azucena, A. D., *Guillén-Fernández*, O., & *Silva-Juárez*, A. (2020). Analog/digital implementation of fractional order chaotic circuits and applications (pp. 41-74). Berlin/Heidelberg, Germany: Springer.
67. Wang, S. F., & Ye, A. (2020). Dynamical properties of fractional-order memristor. Symmetry, 12(3), 437. https://doi.org/10.3390/sym12030437
68. Xu, B., Wang, G., Iu, H. H. C., Yu, S., & Yuan, F. (2019). A memristor-meminductor-based chaotic system with abundant dynamical behaviors. *Nonlinear Dynamics*, 96, 765-788. https://doi.org/10.1007/s11071-019-04820-1
69. Yu, F., Wu, C., Lin, Y., He, S., Yao, W., Cai, S., & Jin, J. (2024). Dynamic analysis and hardware implementation of multi-scroll Hopfield neural networks with three different memristor synapses. *Nonlinear Dynamics*, 1-17. https://doi.org/10.1007/s11071-024-09614-8
70. Zhang, Z., Ushio, T., Zhang, J., Ding, C., & Liu, F. (2020). bifurcation analysis of a class fractional-oder nonlinear Chua's circuit system. *Journal of Advanced Computational Intelligence and Intelligent Informatics*, 24(4), 549-556. https://doi.org/10.20965/jaciii.2020.p0549

[1] Department of Engineering Mathematics and Physics, Faculty of Engineering, Damietta University, New Damietta, 34517, Egypt
Email address: hagarsalman@du.edu.eg

[2] Department of Engineering Mathematics and Physics, Faculty of Engineering, Mansoura University, Mansoura, 35516, Egypt
Email address: abass_hassan@mans.edu.eg

[3] Faculty of Engineering, Mansoura National University, Gamasa, 7731168, Egypt
Email address: fatma_kamal@mans.edu.eg